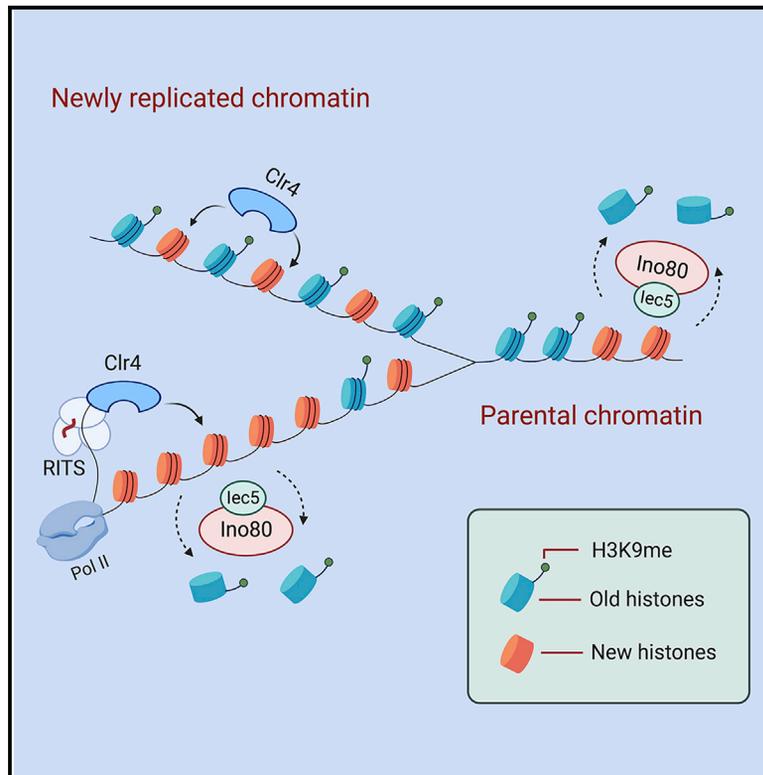# The INO80 Complex Regulates Epigenetic Inheritance of Heterochromatin

Graphical Abstract

Authors

Chun-Min Shan, Kehan Bao, Jolene Diedrich, Xiao Chen, Chao Lu, John R. Yates III, Songtao Jia

Correspondence

songtao.jia@columbia.edu

In Brief

Shan et al. report that the INO80 chromatin-remodeling complex regulates heterochromatin inheritance in wild-type cells and RNAi mutants. Further characterization of the INO80 complex demonstrates that the Iec5 subunit counteracts heterochromatin inheritance through regulating histone turnover but not nucleosome positioning at heterochromatin during DNA replication.

Highlights

- Mutations of INO80 subunits bypass RNAi for pericentric heterochromatin formation

- INO80 counteracts heterochromatin inheritance through its Iec5 subunit

- Iec5 regulates histone turnover, but not nucleosome positioning, at heterochromatin

- Low histone turnover during DNA replication ensures heterochromatin inheritance

CellPress

Article

The INO80 Complex Regulates Epigenetic Inheritance of Heterochromatin

Chun-Min Shan,[1] Kehan Bao,[1] Jolene Diedrich,[2] Xiao Chen,[3] Chao Lu,[3,4] John R. Yates III,[2] and Songtao Jia[1,5,*]

[1]Department of Biological Sciences, Columbia University, New York, NY 10027, USA
[2]Department of Chemical Physiology, The Scripps Research Institute, La Jolla, CA 92037, USA
[3]Department of Genetics and Development, Columbia University Irving Medical Center, New York, NY 10032, USA
[4]Herbert Irving Comprehensive Cancer Center, Columbia University Irving Medical Center, New York, NY 10032, USA
[5]Lead Contact
*Correspondence: songtao.jia@columbia.edu
https://doi.org/10.1016/j.celrep.2020.108561

SUMMARY

One key aspect of epigenetic inheritance is that chromatin structures can be stably inherited through generations after the removal of the signals that establish such structures. In fission yeast, the RNA interference (RNAi) pathway is critical for the targeting of histone methyltransferase Clr4 to pericentric repeats to establish heterochromatin. However, pericentric heterochromatin cannot be properly inherited in the absence of RNAi, suggesting the existence of mechanisms that counteract chromatin structure inheritance. Here, we show that mutations of components of the INO80 chromatin-remodeling complex allow pericentric heterochromatin inheritance in RNAi mutants. The ability of INO80 to counter heterochromatin inheritance is attributed to one subunit, Iec5, which promotes histone turnover at heterochromatin but has little effects on nucleosome positioning at heterochromatin, gene expression, or the DNA damage response. These analyses demonstrate the importance of the INO80 chromatin-remodeling complex in controlling heterochromatin inheritance and maintaining the proper heterochromatin landscape of the genome.

INTRODUCTION

Eukaryotic genomic DNA is folded with histone and non-histone proteins into chromatin. Covalent modifications of histones, chromatin remodeling, and DNA modifications have important roles in setting up the gene expression programs that determine cell identity. Once these chromatin states have been established, they form an epigenetic memory of gene activity that is inherited by subsequent generations of cells (Campos et al., 2014; Moazed, 2011).

Histones have major roles in transmitting epigenetic information (Serra-Cardona and Zhang, 2018; Stewart-Morgan et al., 2020). During DNA replication, the passage of the replication fork disrupts parental nucleosomes. Parental (H3–H4)$_2$ tetramers, which contain original histone modification marks, are deposited at the original location and to both daughter strands to direct the formation of nucleosomes. Because the DNA content increases 2-fold, nucleosomes containing parental (H3–H4)$_2$ cover only half of the replicated DNA. The remaining gaps in the DNA are filled by nucleosomes formed with newly synthesized (H3–H4)$_2$, resulting in the intermingling of nucleosomes containing parental and new (H3–H4)$_2$. The existing histone modifications on parental histones often recruit enzymes responsible for such modifications, leading to modifications of nearby nucleosomes, thereby restoring the original histone modification profiles on both replicated DNA strands. However, the mechanistic details of histone-modification inheritance are still not well understood.

One of the best-studied examples of the inheritance of chromatin states is heterochromatin in the fission yeast *Schizosaccharomyces pombe*. In that organism, large domains of heterochromatin are formed at the pericentric region, subtelomeres, and the silent mating-type region (Grewal and Jia, 2007). The nucleosomes within those regions all contain methylated histone H3 lysine 9 (H3K9me), which is catalyzed by the histone methyltransferase Clr4 (Nakayama et al., 2001; Rea et al., 2000). In addition to the catalytic SET domain, Clr4 contains a chromodomain that binds H3K9me (Zhang et al., 2008). Once Clr4 is recruited to specific genomic loci to initiate H3K9 methylation, repeated cycles of Clr4 binding to H3K9me and the methylation of adjacent nucleosomes on H3K9 leads to the formation of large H3K9me domains. Such a self-propagating mechanism is also proposed to aid the restoration of H3K9me during DNA replication, with parental histones containing H3K9me serving as seeds for the restoration of the entire H3K9me domain (Allshire and Madhani, 2018; Zhang et al., 2008).

The RNA interference (RNAi) pathway is critical for the recruitment of Clr4 to repetitive DNA elements to establish heterochromatin (Grewal and Jia, 2007; Martienssen and Moazed, 2015). The DNA repeats are transcribed, producing double-stranded RNAs (dsRNAs) with the help of an RNA-dependent RNA polymerase complex (RDRC). The ribonuclease Dicer (Dcr1) processes those dsRNAs into small

interfering RNAs (siRNAs), which are loaded onto the RNAi-induced transcriptional silencing complex (RITS) with the help of the Argonaute siRNA chaperone complex (ARC). The Argonaute protein (Ago1) within RITS binds siRNAs and targets RITS to nascent RNA transcripts from repeat regions. RITS then recruits the CLRC complex, which contains the H3K9 methyltransferase Clr4 to initiate H3K9me. H3K9me recruits chromodomain proteins Swi6 and Chp2, which in turn recruit the SHREC complex containing histone deacetylase Clr3 and chromatin-remodeling protein Mit1 to achieve transcriptional silencing.

At the silent mating-type region, heterochromatin persists after removal of RNAi components or the *cenH* repeat sequence that initiates RNAi, consistent with the idea that heterochromatin can be inherited through mitosis without the initiation signal (Grewal and Klar, 1996; Hall et al., 2002). However, such an explanation is complicated by the presence of an additional, albeit less-robust, mechanism of heterochromatin nucleation involving DNA binding proteins Atf1/Pcr1, which cooperates with RNAi to recruit Clr4 to the silent mating-type region (Jia et al., 2004; Wang and Moazed, 2017). To avoid complications from possible unknown mechanisms at endogenous heterochromatin loci, ectopic heterochromatin is established by the recruitment of Clr4 to *tetO* binding sites through a TetR-Clr4 fusion protein (Audergon et al., 2015; Ragunathan et al., 2014). This ectopic heterochromatin is unable to maintain itself after the addition of tetracycline to remove TetR-Clr4 from *tetO*. Therefore, it seems that cells have mechanisms that prevent histone-based heterochromatin maintenance. Indeed, removal of a JmjC domain protein Epe1 allows the inheritance of this artificial heterochromatin established by TetR-Clr4 even after TetR-Clr4 release (Audergon et al., 2015; Ragunathan et al., 2014). Epe1 is a putative H3K9 demethylase, and it is suggested that active H3K9me removal by Epe1 prevents epigenetic inheritance. However, the enzymatic activity of Epe1 has not been demonstrated *in vitro*, and the commonly used mutations that are expected to abolish Epe1 demethylase activity actually influence heterochromatin through non-enzymatic functions (Raiymbek et al., 2020). Therefore, the mechanisms that prevent histone-based heterochromatin maintenance in fission yeast remain unclear.

At pericentric repeats, heterochromatin is not properly maintained in RNAi mutants, even though RNAi is expected to be only required for heterochromatin establishment but not its subsequent maintenance (Kagansky et al., 2009; Ragunathan et al., 2014). We hypothesized that if there are pathways that actively prevent heterochromatin maintenance, inactivating such pathways will allow heterochromatin to be inherited, even in the absence of RNAi. We, therefore, performed a genetic screen for mutations that allow pericentric heterochromatin inheritance in RNAi mutants (Tadeo et al., 2013). Here, we describe the identification and characterization of mutations of components of the INO80 chromatin-remodeling complex in regulating heterochromatin inheritance. All the mutations identified regulate the stability of one INO80 subunit Iec5, and *iec5Δ* does not affect nucleosome positioning but affects histone turnover at heterochromatin. This separation-of-function mutation allows us to demonstrate that INO80 promotes histone turnover to

regulate epigenetic inheritance and the heterochromatin landscape across the genome.

RESULTS

Mutations of the INO80 Chromatin Remodeling-Complex Rescue Pericentric Heterochromatin Defects of RNAi Mutants

In fission yeast, heterochromatin integrity can be conveniently measured by the silencing of reporter genes inserted within heterochromatin. For example, a *ura4+* reporter gene inserted at the outer repeat region of centromere I (*otr::ura4+*) is silenced, leading to robust cell growth on medium containing 5-fluoroorotic acid (FOA), which is toxic to cells expressing *ura4+* (Allshire et al., 1995). Mutations that compromise heterochromatin, such as *dcr1Δ*, which deletes a gene encoding the ribonuclease Dicer responsible for generating siRNAs, leads to *otr::ura4+* silencing defects and little growth on FOA-containing medium. We have previously introduced the *otr::ura4+* reporter and *dcr1Δ* into the fission yeast-deletion library to identify mutations that allow for heterochromatin inheritance in the absence of RNAi (Figure 1A) (Tadeo et al., 2013). The screen also identified three additional mutations, *iec1Δ*, *hap2Δ*, and *nht1Δ*, which harbor deletions of genes whose products are annotated as components of the INO80 chromatin-remodeling complex (Figure 1B). The subunits that make up the catalytic core of the INO80 chromatin-remodeling complex, including Ino80, Rvb1, Rvb2, Ies2, Ies4, Ies6, Act1, Arp4, Arp5, Arp8, and Taf14, are conserved across species (Morrison and Shen, 2009). Organisms analyzed so far all contain species-specific accessory subunits. The three mutations that we identified are all accessory subunits of the fission yeast INO80 complex (Hogan et al., 2010), and we did not identify any subunits of the conserved INO80 core subunits in our screen.

To confirm those findings, we generated an *nht1Δ dcr1Δ otr::ura4+* strain. Serial dilution analyses show that these cells indeed grow robustly on FOA-containing medium (Figure 1C). In addition, chromatin immunoprecipitation (ChIP) analyses show that levels of H3K9me3 and Swi6 levels at pericentric *dh* repeats are reduced in *dcr1Δ* cells but are improved in *nht1Δ dcr1Δ* cells (Figure 1D). Furthermore, *dh* transcripts levels are reduced in *nht1Δ dcr1Δ* compared with *dcr1Δ* cells (Figure 1D). Therefore, *nht1Δ dcr1Δ* not only improves silencing of the *otr::ura4+* reporter but also restores heterochromatin mark levels at pericentric repeats, even though heterochromatin is not restored to wild-type levels.

Pericentric heterochromatin is responsible for the recruitment of high levels of cohesin to aid the accurate segregation of chromosomes during mitosis (Bernard et al., 2001; Nonaka et al., 2002). When pericentric heterochromatin is compromised, such as in a *dcr1Δ* strain, the levels of cohesion at pericentric repeats are reduced, and centromeres are defective in attaching to microtubules for biorientation (Hall et al., 2003; Volpe et al., 2003). As a result, these cells are very sensitive to the microtubule poison thiabendazole (TBZ). We found that, in *nht1Δ dcr1Δ* cells, levels of cohesion subunit Rad21 are higher than in *dcr1Δ* cells (Figure 1D). Moreover, *nht1Δ dcr1Δ* cells are not as sensitive to TBZ as *dcr1Δ* cells are (Figure 1C). These results
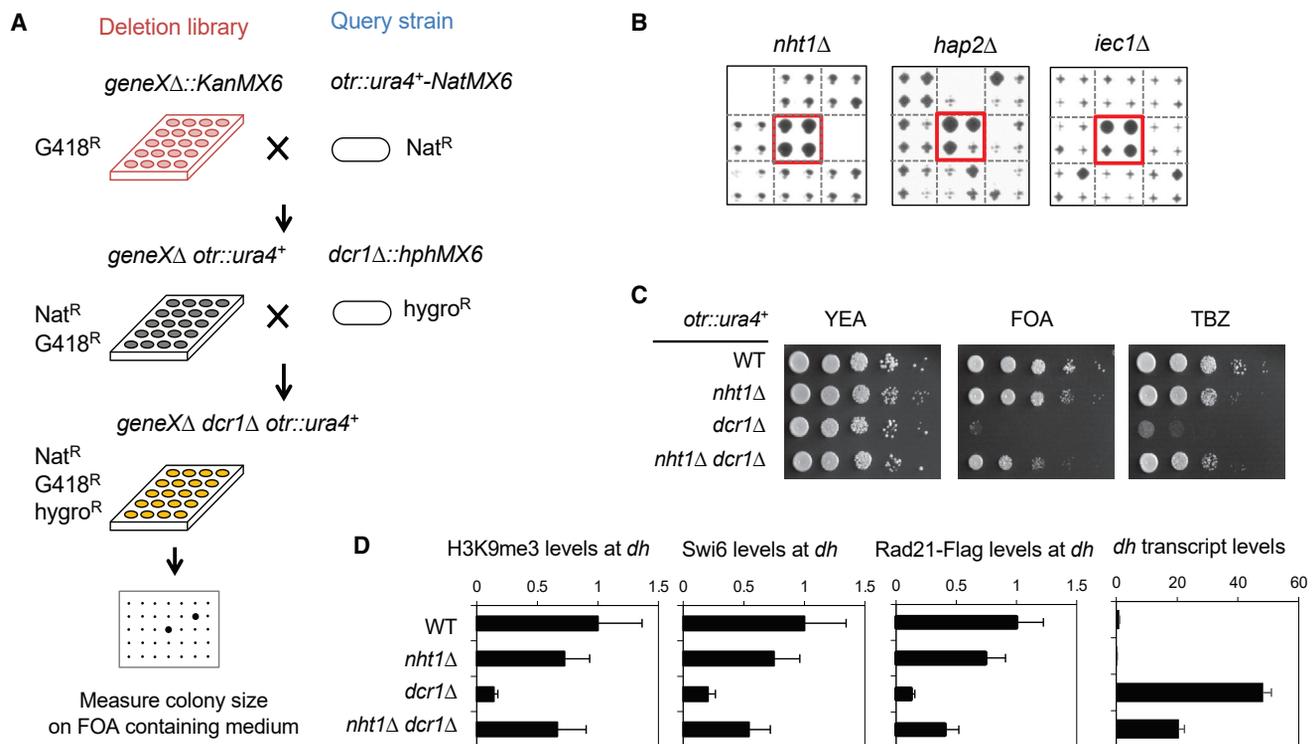
Figure 1. Identification of INO80 Complex Components as Regulators of Heterochromatin Inheritance

(A) Schematic diagram of the screen with the fission yeast-deletion library for mutations that allow *otr::ura4+* silencing to be inherited in a *dcr1Δ* background.

(B) Images of sections of cells grown on medium containing 5-FOA. Each square represents quadruplicates of one gene deletion. Red boxes highlight the identified mutations.

(C) Serial dilution analyses of the indicated strains to measure the expression of *otr::ura4+* and sensitivity to TBZ.

(D) ChIP qPCR analyses of H3K9me3, Swi6, and Rad21-FLAG levels at pericentric *dh* repeats, normalized to *act1+*, and qRT-PCR analyses of *dh* transcript levels, normalized to *act1+*. Data are presented as means ± SD, n = 3.

demonstrate that *nht1Δ dcr1Δ* cells also restore functional pericentric heterochromatin.

INO80 Mutants Bypass RNAi, but Not Histone Modification Pathways, for Pericentric Heterochromatin Inheritance

Heterochromatin formation at pericentric repeats requires a large number of proteins that can be divided into two main categories: RNAi, which is required for the initial targeting of Clr4 to repeats to establish heterochromatin, and histone modifications, which are required for both heterochromatin establishment and maintenance (Figure 2A). Dilution analyses show that *nht1Δ* rescues pericentric silencing defects and TBZ sensitivity of mutants involved in RNAi, including the deletions of RITS components *ago1Δ* and *chp1Δ*, ARC complex component *arb1Δ*, and RDRC component *rdp1Δ* (Figure 2B). However, *nht1Δ* does not rescue silencing defects and TBZ sensitivity of mutants involved in histone modifications, such as CLRC complex components *clr4Δ* and *rik1Δ*, HP1 proteins *swi6Δ* and *chp2Δ*, and SHREC complex components *clr3Δ* and *mit1Δ* (Figure 2C).

To further examine whether *nht1Δ dcr1Δ* rescues heterochromatin establishment or maintenance, we used genetic crosses to introduce *otr::ura4+* into *nht1Δ dcr1Δ* cells from either a

silenced state (from wild-type cells) to measure heterochromatin maintenance, or an activated state (from *clr4Δ* cells) to measure heterochromatin establishment (Figure 2D). It has been shown that *dcr1Δ* cells failed to establish heterochromatin in both establishment and maintenance crosses (Bayne et al., 2010; Hall et al., 2002). Interestingly, *nht1Δ dcr1Δ* cells only efficiently silence *otr::ura4+* if it is inherited from a wild-type cell (maintenance), but fail to silence *otr::ura4+* if it is inherited from a *clr4Δ* cell (establishment) (Figure 2E). ChIP analyses of H3K9me3 levels at *otr::ura4+* also confirm that conclusion (Figure 2E). These results suggest that *nht1Δ* facilitates inheritance of preexisting heterochromatin in RNAi mutants but cannot establish heterochromatin *de novo* in the absence of RNAi.

Characterization of the INO80 Complex

To determine whether the accessory subunits function solely as part of the INO80 complex, we generated FLAG-tagged versions of Ino80, Nht1, Iec1, Hap2, and two additional factors, Iec3 and Iec5, which are also annotated as accessory INO80 subunits. Affinity purification of these proteins, followed by mass spectrometry analyses, shows that they have the same associated proteins with similar peptide counts and sequence coverage, suggesting that all five proteins are exclusively in the INO80 complex (Figure 3A).
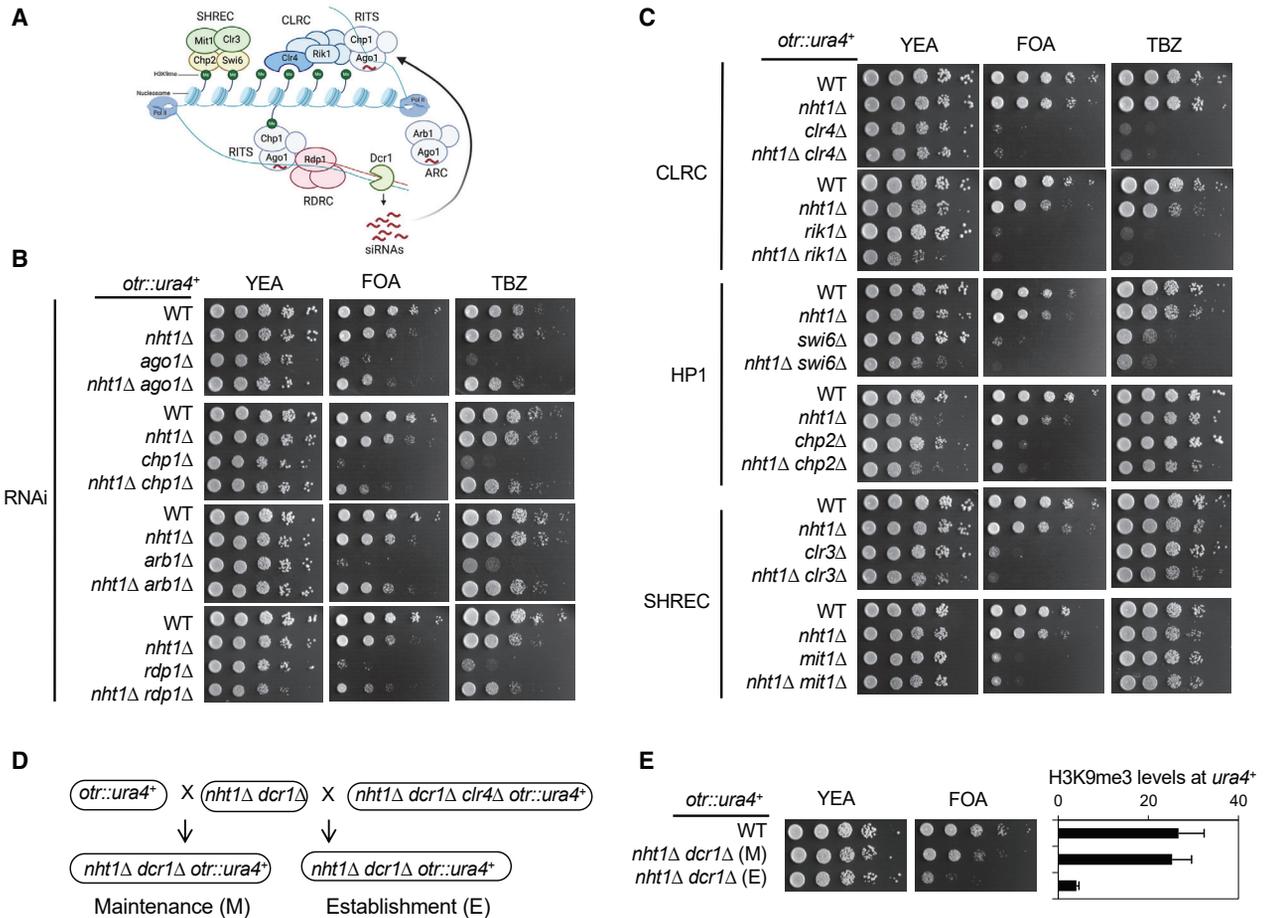
Figure 2. Genetic Interactions of INO80 Mutants with Heterochromatin Mutants

(A) Schematic diagram of RNAi-mediated heterochromatin assembly. RITS, RDRC, Arb1, and Dcr1 are involved in RNAi and the targeting of Clr4 to pericentric repeats. CLRC, Swi6, Chp2, and SHREC are involved in chromatin modifications.

(B and C) Serial dilution analyses of the indicated strains to measure the expression of $otr::ura4^+$ and sensitivity to TBZ. Note that $chp2\varDelta$, $clr3\varDelta$, and $mit1\varDelta$ are not sensitive to TBZ.

(D) Schematic diagram of establishment and maintenance crosses.

(E) Left, serial dilution analyses of indicated strains to measure the expression of $otr::ura4^+$. Right, ChIP analysis of H3K9me3 levels at $otr::ura4^+$, normalized to $act1^+$. Data are presented as means ± SD, n = 3.

We then constructed double mutants of $dcr1\varDelta$ with individual INO80 component mutations and examined their effects on the silencing of $otr::ura4^+$. Interestingly, we found that mutations of every accessory subunit of INO80, such as $iec1\varDelta$, $hap2\varDelta$, $iec3\varDelta$, and $iec5\varDelta$, alleviate $otr::ura4^+$ silencing defects in $dcr1\varDelta$ cells (Figure 3B). We did not identify $iec3\varDelta$ or $iec5\varDelta$ in our screen because the $iec3\varDelta$ in the fission yeast-deletion library is incorrect, and $iec5\varDelta$ is not present in the library. None of the tested mutations of the conserved subunits, such as $ies2\varDelta$, $ies4\varDelta$, or $arp8\varDelta$, alleviates silencing defects of $dcr1\varDelta$, consistent with the fact that these mutations were not identified in our screen (Figure 3C). Other conserved mutations of the INO80 complex are either lethal or extremely sick for further characterization.

Among all chromatin-remodeling proteins, Ino80 shares sequence similarity with Swr1, which catalyzes the incorporation of histone H2A variant H2A.Z into chromatin (Mizuguchi et al., 2004). We found that $swr1\varDelta$ $dcr1\varDelta$ cells are still defective in

the silencing of $otr::ura4^+$ and TBZ sensitive, similar to $dcr1\varDelta$ cells (Figure 3C). In addition, ChIP analyses show that Pht1, the fission yeast H2A.Z, is not enriched at pericentric repeats (Figure S1A), consistent with previous analyses (Zofall et al., 2009). Moreover, $nht1\varDelta$ has no effects on the localization of Pht1 at pericentric repeats or the $vid21^+$ gene promoter. In contrast, $swr1\varDelta$ abolished Pht1 at the $vid21^+$ gene promoter but has no effects on Pht1 levels at the pericentric repeats (Figure S1A) (Hou et al., 2010). Moreover, the silencing of $otr::ura4^+$ is maintained in $swr1\varDelta$ $nht1\varDelta$ $dcr1\varDelta$ cells (Figure S1B). These results suggest that the ability of INO80 mutants to rescue RNAi is unlikely through regulating H2A.Z localization.

Characterization of the Accessory Subunits of the INO80 Complex

To further analyze the role of the accessory subunits in regulating INO80 complex function, we performed affinity purification of

A

| protein	Ino80-Flag		Iec1-Flag		Hap2-Flag		Nht1-Flag		Iec3-Flag		Iec5-Flag	
	peptide	coverage	peptide	coverage	peptide	coverage	peptide	coverage	peptide	coverage	peptide	coverage
Ino80 core												
Ino80	276	65.80%	419	75.90%	284	68.00%	249	67.50%	378	71.00%	370	70.20%
Rvb1	132	78.90%	244	92.50%	138	80.70%	125	81.80%	218	78.70%	189	76.10%
Rvb2	120	79.10%	207	95.70%	134	79.60%	114	82.40%	178	85.20%	169	87.50%
Ies2	43	46.80%	77	51.50%	55	51.20%	52	51.20%	73	51.50%	69	51.50%
Arp8	131	78.10%	217	86.60%	148	81.60%	130	74.30%	215	85.60%	225	87.50%
Act1	73	78.90%	129	89.90%	73	82.90%	68	86.90%	120	85.90%	103	82.40%
Arp4	67	84.50%	119	90.10%	80	91.20%	78	84.10%	119	91.50%	117	93.50%
Tfg3	53	80.10%	67	81.30%	49	80.90%	52	83.40%	69	73.90%	55	63.50%
Ies4	36	64.40%	47	73.20%	32	64.40%	33	73.20%	52	73.20%	50	58.20%
Arp5	123	73.80%	237	84.60%	153	77.90%	130	76.80%	234	83.20%	258	78.80%
Ies6	22	70.90%	31	77.80%	23	70.90%	18	70.90%	27	70.90%	35	77.80%
Accessory												
Iec1	41	52.60%	66	62.20%	47	53.00%	42	52.60%	51	53.00%	63	60.20%
Hap2	12	46.80%	11	53.20%	15	32.50%	10	32.50%	11	53.20%	18	54.50%
Nht1	63	56.90%	129	70.70%	76	58.70%	91	63.60%	136	71.00%	133	70.70%
Iec3	27	46.40%	32	53.00%	28	51.80%	27	51.80%	34	58.30%	34	53.00%
Iec5	22	44.40%	38	69.40%	29	68.80%	24	69.40%	39	69.40%	48	69.40%
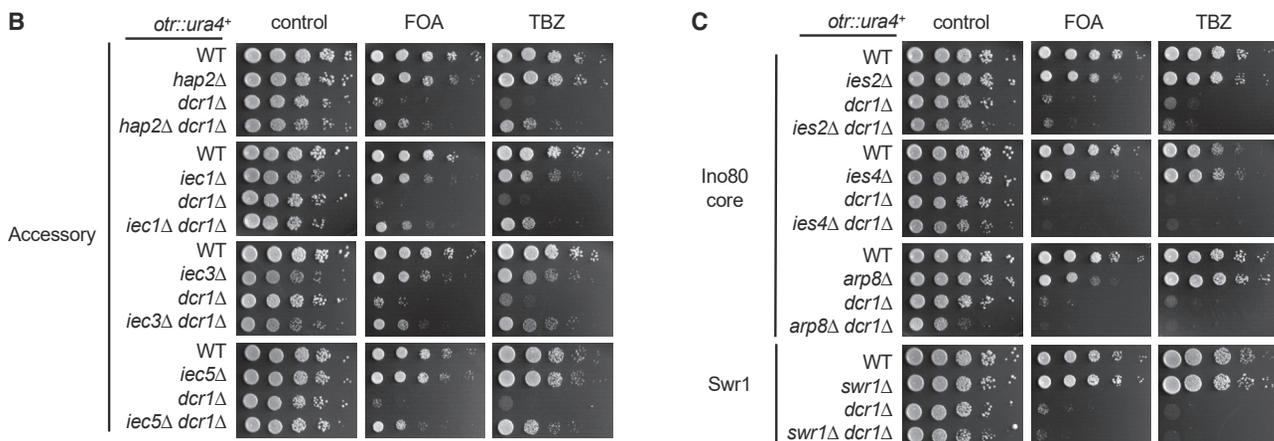
Figure 3. Characterization of the Role of the Individual Subunit of the INO80 Complex in Heterochromatin Inheritance

(A) Mass spectrometry analyses of affinity-purified INO80 complex components. The number of peptides identified and the percentage of each protein those peptides cover are indicated.

(B and C) Serial dilution analyses of indicated strains to measure the expression of *otr::ura4+* and sensitivity to TBZ.

See also Figure S1.

Ino80-FLAG in *iec1Δ*, *hap2Δ*, *nht1Δ*, *iec3Δ*, and *iec5Δ* cells. Mass spectrometry analyses show that *iec1Δ* or *hap2Δ* results in the loss of association of all accessory subunits from the INO80 complex (Figure 4A). In addition, *nht1Δ* or *iec3Δ* results in the loss of Nht1, Iec3, and Iec5 from the INO80 complex but have no effect on the association of Iec1 or Hap2 with Ino80. Finally, *iec5Δ* results in the loss of only Iec5 from the INO80 complex, but it has no effect on the association of any other accessory subunits with Ino80, suggesting that the effect of mutating other accessory subunits of the INO80 complex on heterochromatin silencing is likely due to a loss of Iec5 subunit of INO80 complex.

To examine the functions of the accessory subunits, we performed RNA sequencing (RNA-seq) analyses of RNA purified from *iec1Δ*, *nht1Δ*, and *iec5Δ* cells. We found that all three mutations mildly affect gene expression, with *iec1Δ* having a stron-ger effect than *nht1Δ*, which has a stronger effect than *iec5Δ* has (Figures 4B and 4C; Tables S1–S6). In addition, *iec1Δ*, *hap2Δ*, *nht1Δ*, and *iec3Δ* cells are highly sensitive to DNA-damage reagent bleomycin, but *iec5Δ* cells are less sensitive (Figure 4D). The severity of effects on gene expression or bleomycin sensitivity is consistent with the mass spectrometry results. Importantly, *iec5Δ* has almost no effect on transcription programs, and none of the affected genes are involved in heterochromatin assembly. Therefore, the effects of *iec5Δ* on heterochromatin are unlikely to be due to indirect effects on the transcription of genes involved in heterochromatin inheritance.

Iec5 Is the Critical Component of the INO80 Complex in Regulating Heterochromatin Inheritance

Our results suggest that Iec1 and Hap2 are in close contact with the INO80 catalytic core, Nht1 and Iec3 are linked to
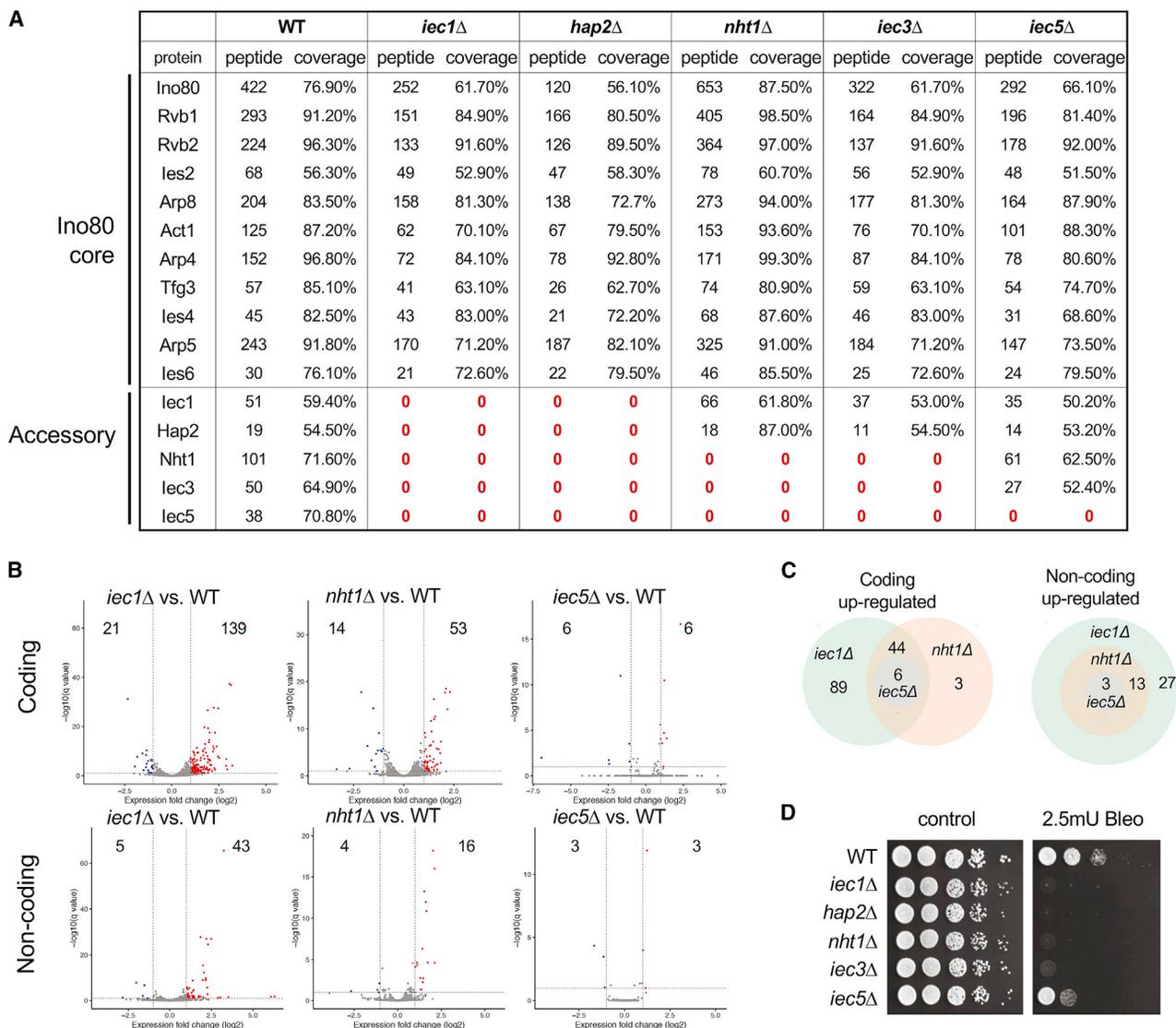
A

	protein	WT peptide	WT coverage	iec1Δ peptide	iec1Δ coverage	hap2Δ peptide	hap2Δ coverage	nht1Δ peptide	nht1Δ coverage	iec3Δ peptide	iec3Δ coverage	iec5Δ peptide	iec5Δ coverage
Ino80 core	Ino80	422	76.90%	252	61.70%	120	56.10%	653	87.50%	322	61.70%	292	66.10%
	Rvb1	293	91.20%	151	84.90%	166	80.50%	405	98.50%	164	84.90%	196	81.40%
	Rvb2	224	96.30%	133	91.60%	126	89.50%	364	97.00%	137	91.60%	178	92.00%
	Ies2	68	56.30%	49	52.90%	47	58.30%	78	60.70%	56	52.90%	48	51.50%
	Arp8	204	83.50%	158	81.30%	138	72.7%	273	94.00%	177	81.30%	164	87.90%
	Act1	125	87.20%	62	70.10%	67	79.50%	153	93.60%	76	70.10%	101	88.30%
	Arp4	152	96.80%	72	84.10%	78	92.80%	171	99.30%	87	84.10%	78	80.60%
	Tfg3	57	85.10%	41	63.10%	26	62.70%	74	80.90%	59	63.10%	54	74.70%
	Ies4	45	82.50%	43	83.00%	21	72.20%	68	87.60%	46	83.00%	31	68.60%
	Arp5	243	91.80%	170	71.20%	187	82.10%	325	91.00%	184	71.20%	147	73.50%
	Ies6	30	76.10%	21	72.60%	22	79.50%	46	85.50%	25	72.60%	24	79.50%
Accessory	Iec1	51	59.40%	0	0	0	0	66	61.80%	37	53.00%	35	50.20%
	Hap2	19	54.50%	0	0	0	0	18	87.00%	11	54.50%	14	53.20%
	Nht1	101	71.60%	0	0	0	0	0	0	0	0	61	62.50%
	Iec3	50	64.90%	0	0	0	0	0	0	0	0	27	52.40%
	Iec5	38	70.80%	0	0	0	0	0	0	0	0	0	0

Figure 4. Characterization of the Accessory Subunits of INO80

(A) Mass spectrometry analyses of affinity-purified Ino80-FLAG from different backgrounds. The number of peptides identified and the percentage of each protein those peptides cover are indicated.

(B) Volcano plots of differentially expressed coding (top) or non-coding genes (bottom) in INO80 mutants compared with wild type. Thresholds of 2-fold change and q < 0.1 are used. The q value is the false-discovery-rate-adjusted p value. Red dots indicate RNA with more than a 2-fold increase, and blue dots indicate RNA with more than a 2-fold decrease.

(C) Venn diagram showing the overlaps of RNA that are downregulated in different INO80 complex mutants.

(D) Serial dilution analyses of indicated strains to measure sensitivity to bleomycin.

See also Tables S1–S6.

INO80 catalytic core through Iec1 and Hap2, and Iec5 is linked to INO80 catalytic core through Nht1 and Iec3 (Figure 5A). Interestingly, western blot analyses show that Iec5 is less stable in iec1Δ, hap2Δ, nht1Δ, and iec3Δ cells (Figure 5B), suggesting that the association of Iec5 with the INO80 catalytic core is required for Iec5 stability and that the effect of iec1Δ, hap2Δ, nht1Δ, and iec3Δ on heterochromatin is through regulating Iec5 stability. To test whether that was the case, we generated a strain expressing Iec1 with a GBP (GFP binding protein) tag (Rothbauer et al., 2008) and Iec5 with a GFP tag. The interaction between GBP and GFP is expected to tether Iec5 back to the INO80 complex, even in the absence of Nht1 or Iec3 (Figure 5C). Iec5-GFP shows a nuclear signal, which is lost in nht1Δ cells (Figure 5D), consistent with the western blot analysis. Interestingly, Iec5-GFP signal is restored in nht1Δ Iec1-GBP cells (Figure 5D). Moreover, nht1Δ dcr1Δ iec5-GFP iec1-GBP cells cannot silence otr::ura4⁺ and are sensitive to TBZ.
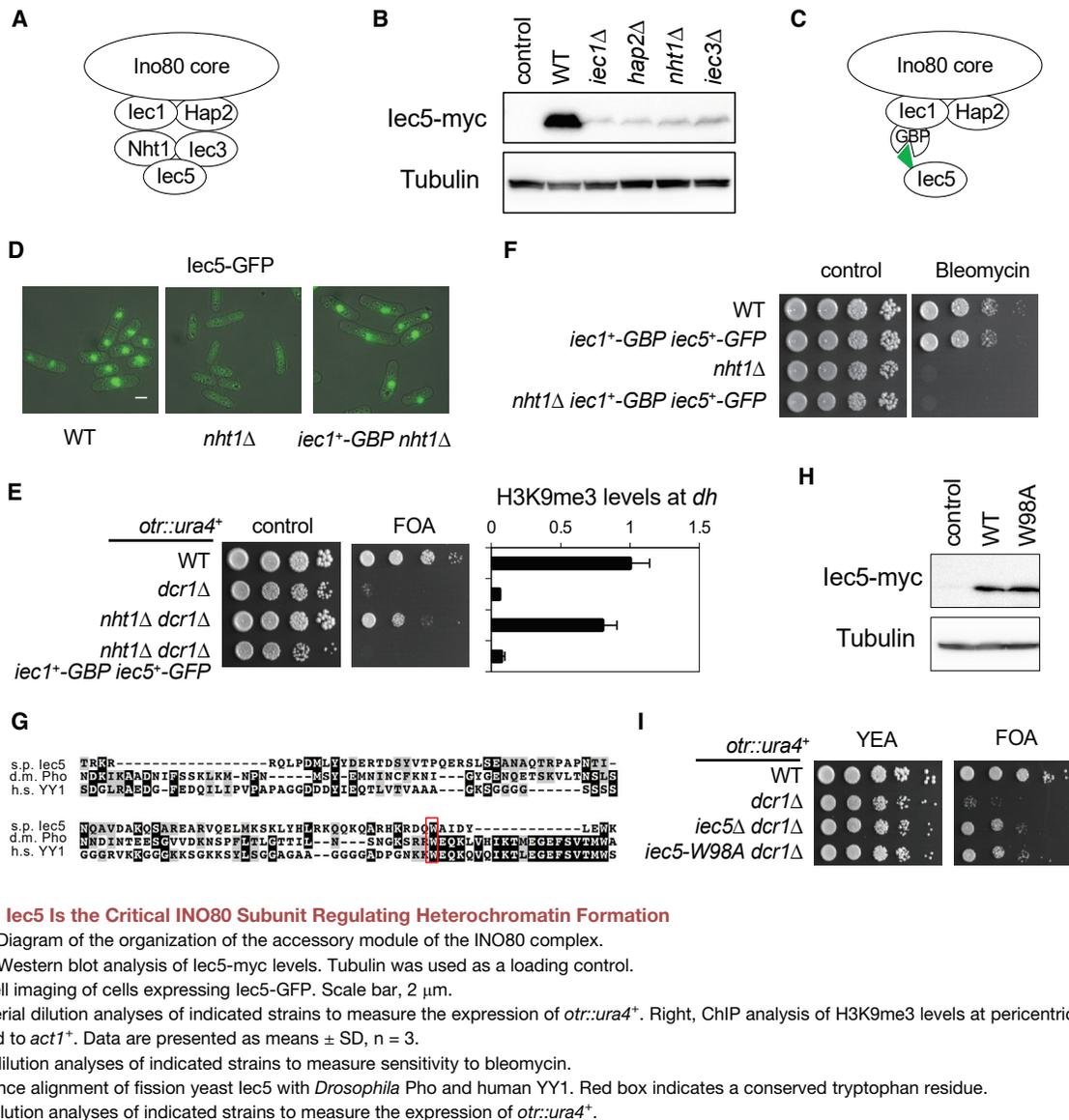
Figure 5. Iec5 Is the Critical INO80 Subunit Regulating Heterochromatin Formation
(A and C) Diagram of the organization of the accessory module of the INO80 complex.
(B and H) Western blot analysis of Iec5-myc levels. Tubulin was used as a loading control.
(D) Live cell imaging of cells expressing Iec5-GFP. Scale bar, 2 μm.
(E) Left, serial dilution analyses of indicated strains to measure the expression of $otr::ura4^+$. Right, ChIP analysis of H3K9me3 levels at pericentric dh repeats, normalized to $act1^+$. Data are presented as means ± SD, n = 3.
(F) Serial dilution analyses of indicated strains to measure sensitivity to bleomycin.
(G) Sequence alignment of fission yeast Iec5 with *Drosophila* Pho and human YY1. Red box indicates a conserved tryptophan residue.
(I) Serial dilution analyses of indicated strains to measure the expression of $otr::ura4^+$.

Furthermore, ChIP analyses show that H3K9me3 is abolished from pericentric repeats in these cells (Figure 5E). These results suggest that the dissociation of Iec5 from INO80 is critical for the restoration of heterochromatin in RNAi mutant cells. Cells containing $nht1\Delta$ $iec5$-GFP $iec1$-GBP are still sensitive to bleomycin, similar to $nht1\Delta$ cells (Figure 5F), suggesting that the function of Nht1/Iec3 in regulating the DNA damage response is independent of the association of Iec5 with Ino80, and such functions are not involved in heterochromatin regulation.

Although no clear homologs of Iec5 have been identified in higher organisms, Iec5 shows sequence homology with components of the INO80 complex from other organisms, such as human YY1 and fruit fly Pho (Figure 5G). Mutation of a conserved tryptophan residue in Iec5 (Iec5-W98A), which has no effects on Iec5 protein levels, restores silencing of $otr::ura4^+$ in $dcr1\Delta$

cells, similar to $iec5\Delta$ (Figures 5H and 5I). Therefore, higher organisms might have evolved functional counterparts of Iec5 into other proteins of the INO80 complex.

Iec5 Regulates Histone Turnover at Heterochromatin
Mass spectrometry analyses of proteins associated with heterochromatin components repeatedly identify the INO80 complex, and ChIP analyses show that INO80 complex components can be detected at pericentric repeats, suggesting that the INO80 complex functions directly at heterochromatin (Fischer et al., 2009; Iglesias et al., 2020; Motamedi et al., 2008; Singh et al., 2020). Indeed, our co-immunoprecipitation analysis of proteins associated with FLAG-Swi6 shows the presence of Nht1-myc (Figure 6A). Moreover, ChIP analysis shows that low levels of Ino80-FLAG are enriched at pericentric dh repeats, and its localization is not affected in $clr4\Delta$ (Figure 6B). However, $iec5\Delta$ has no
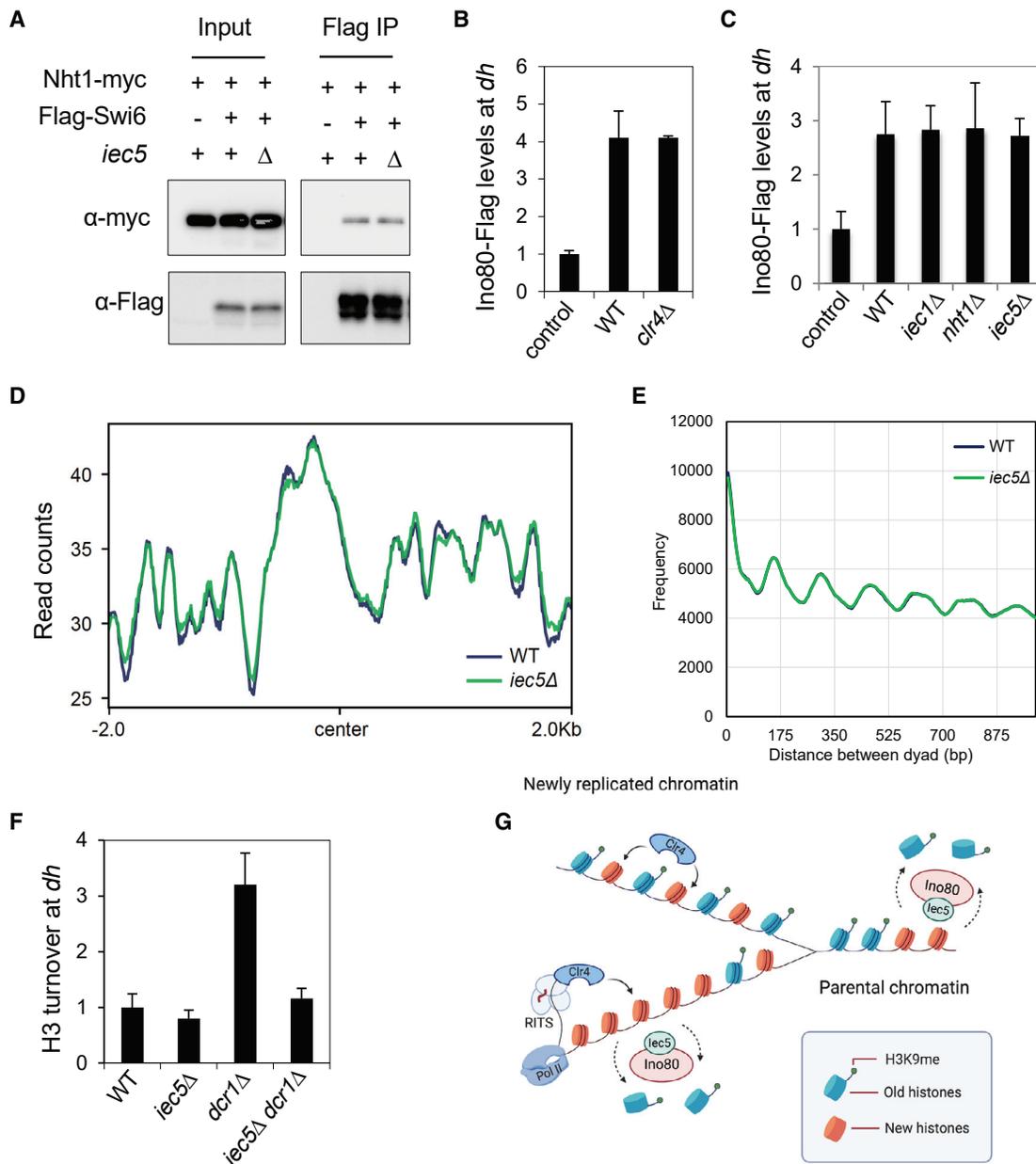
Figure 6. Iec5 Regulates Histone Turnover but Not Nucleosome Positioning at Pericentric Heterochromatin

(A) Co-immunoprecipitation analysis of FLAG-Swi6 and Nht1-myc. Immunoprecipitation was performed with a FLAG antibody, and western blots were performed with Myc and FLAG antibodies.

(B and C) ChIP analysis of Ino80-FLAG levels at pericentric *dh* repeats. Data are presented as means ± SD, n = 3.

(D) Nucleosome positioning within the pericentric repeat region as measured by MNase-seq. The x axis shows the position relative to the center of the pericentric repeat annotated feature. The y axis shows the normalized read counts (counts per million [CPM]). Data are the averages of two independent experiments.

(E) Phasogram of nucleosomes within the pericentric repeat region. The x axis shows the range of recorded phases. The y axis shows the frequencies of the corresponding phases. Data are the averages of two independent experiments.

(F) ChIP analysis of H3-FLAG levels at pericentric *dh* repeats. Data are presented as means ± SD, n = 3.

(G) A model for the role of the INO80 complex in heterochromatin inheritance during DNA replication. INO80 increases the rate of histone turnover, reducing the amounts of parental histones containing H3K9me. Therefore, RNAi-mediated recruitment of Clr4 is required to counter such dilution effects to maintain heterochromatin.

See also Figures S2 and S3.

effects on Swi6-Nht1 association and does not affect the localization of Ino80-FLAG to *dh* repeats (Figures 6A and 6C). Therefore, Iec5 is not required for the recruitment of the INO80 complex to heterochromatin.

One of the key activities of the INO80 complex is to regulate nucleosome positioning (Krietenstein et al., 2016; Udugama et al., 2011; Yen et al., 2012). To test whether Iec5 is required for nucleosome positioning at heterochromatin, we performed micrococcal nuclease digestion with deep sequencing (MNase-seq) analysis to map nucleosome positions. However, *iec5Δ* or *iec5Δ dcr1Δ* has little effect on the positioning of nucleosomes at pericentric repeats compared with wild-type or *dcr1Δ* cells, respectively (Figures 6D, 6E, and S2).

INO80 also regulates histone turnover (Singh et al., 2020; Yen et al., 2013). To further examine the role of Iec5 in regulating histone turnover at heterochromatin, we used a strain in which H3-FLAG is under the control of the *urg1* promoter at the endogenous *urg1*+ locus, which can be quickly induced by the addition of uracil in the growth medium (Wang et al., 2015). We used hydroxyurea (HU) to block cells from entering the cell cycle and thereby preventing replication-coupled histone incorporation before the induction of H3-FLAG. We then used ChIP to measure the incorporation of FLAG-H3 into chromatin as an indication of histone turnover. We found that the enrichment of H3-FLAG at pericentric repeats is low in wild-type cells but increases in *dcr1Δ* cells, suggesting that histone turnover increases in RNAi mutants, consistent with previous findings (Figure 6F) (Aygün et al., 2013; Wang et al., 2015). In *iec5Δ dcr1Δ* and *nht1Δ dcr1Δ* cells, H3-FLAG turnover is reduced compared with *dcr1Δ* cells (Figures 6F and S3A). Moreover, using Iec1-GFP and Iec5-GFP to reconnect Iec5 to the INO80 complex leads to greater histone turnover in *nht1Δ dcr1Δ* cells (Figure S3A). Finally, INO80 seems to specifically regulate histone turnover at heterochromatin because, in a *clr4Δ* background, which completely abolished heterochromatin, histone turnover in *clr4Δ iec5Δ* is similar to that in *clr4Δ* cells (Figure S3B).

RNAi is required for the initial recruitment of H3K9 methyltransferase Clr4 to pericentric repeats to establish heterochromatin. Once initiated, heterochromatin can be stably propagated through mitosis because of the deposition of parental histones, which serve as seeds to recruit Clr4 to restore H3K9 methylation. We propose that the presence of the INO80 complex at heterochromatin increases histone turnover rates, thereby reducing the amounts of parental histones on replicated DNA to prevent proper epigenetic inheritance (Figure 6G). As a result, RNAi is consistently needed to reestablish heterochromatin to compensate for the loss of parental histones during DNA replication.

Iec5 Regulates Heterochromatin Inheritance and the Heterochromatin Landscape

We then examined the effects of Iec5 on heterochromatin in otherwise wild-type cells. We used a strain in which the SET domain of Clr4 is targeted to 10 copies of *tetO* binding sites through a TetR-Clr4-SET fusion protein (Figure 7A), resulting in the formation of a large heterochromatin domain that silences a neighboring GFP reporter gene (Ragunathan et al., 2014). The addition of tetracycline to the medium leads to the quick release of TetR-Clr4-SET, and heterochromatin can be inherited

through endogenous Clr4, which binds H3K9me through its chromodomain. In wild-type cells, heterochromatin decays quickly, and within 24 h, H3K9me3 is completely lost around *tetO*, accompanied by the strong expression of GFP, which can be measured by fluorescence-activated cell sorting (FACS) (Figures 7B, 7C, and S4A). Removal of the JmjC domain protein Epe1 greatly reduces heterochromatin decay, and after 24 h, H3K9me3 levels are only reduced slightly, and most cells still silence GFP expression. In contrast, *iec5Δ* cells activate GFP expression at a slower rate than wild-type cells do, and H3K9me3 is still detectable at *tetO* binding sites at 24 h (Figures 7B, 7C, and S4A). Moreover, *iec5Δ* has little effects on nucleosome positioning around *tetO* binding sites (Figure S4B) but shows reduced turnover of histone H3 (Figure S4C). These results indicate that Iec5 regulates heterochromatin inheritance through regulating histone turnover in wild-type cells.

To further examine the effects of INO80 on heterochromatin across the genome, we performed ChIP-seq analysis of H3K9me2. In wild-type cells, in addition to large constitutive heterochromatin domains at centromeres, telomeres, and the silent mating-type region, H3K9me2 is also present at a number of loci within euchromatin, termed heterochromatin islands (Figure 7D) (Zofall et al., 2012). Interestingly, *iec5Δ* results in the increase of H3K9me2 levels at most heterochromatin islands that we can detect (Figures 7D and 7E). ChIP-qPCR analysis confirms that H3K9me2 increases at typical heterochromatin islands, such as *mei4*+, *ssm4*+, and *mcp5*+ (Figure S5A).

We then examined the epistasis relationship between *epe1Δ* and *iec5Δ* by generating an *epe1Δ iec5Δ* double mutant. The decay rate of artificial heterochromatin after Clr4 release in *epe1Δ iec5Δ* cells is similar to that of *epe1Δ* cells (Figure S4A). Moreover, ChIP analysis shows that H3K9me2 levels at *mei4*+ are higher in *epe1Δ* cells than in *iec5Δ* cells, and *epe1Δ iec5Δ* cells show no further increase (Figure S5B). These results suggest that Epe1 and INO80 function in the same pathway.

We noticed that the *iec1*+ locus was annotated as a heterochromatin island in *epe1Δ* cells (Figure S6A) (Zofall et al., 2012), raising the possibility that the expression of Iec1 might be affected by *epe1Δ*. However, we found that *epe1Δ* has no effects on *iec1*+ mRNA levels or protein levels (Figures S6B and S6C). We also found that *epe1Δ* has no effects on Iec5 protein levels, and vice versa, *iec5Δ* has no effects on Epe1 protein levels (Figure S6C). Therefore, Epe1 and INO80 function together through mechanisms other than regulating their protein levels.

DISCUSSION

The dogma for epigenetic inheritance is that, during DNA replication, parental histones are equally distributed into two daughter DNA strands, and existing modifications on parental histones then recruit enzymes that catalyze the same modifications to modify neighboring newly synthesized histones (Figure 6G). Such a self-propagating mechanism allows histone modification patterns to be inherited through generations, even long after the initial signals that establish such patterns disappear. In fission yeast, the RNAi pathway is required for the recruitment of the H3K9 methyltransferase Clr4 to pericentric repeats to establish heterochromatin. However, RNAi mutants cannot maintain
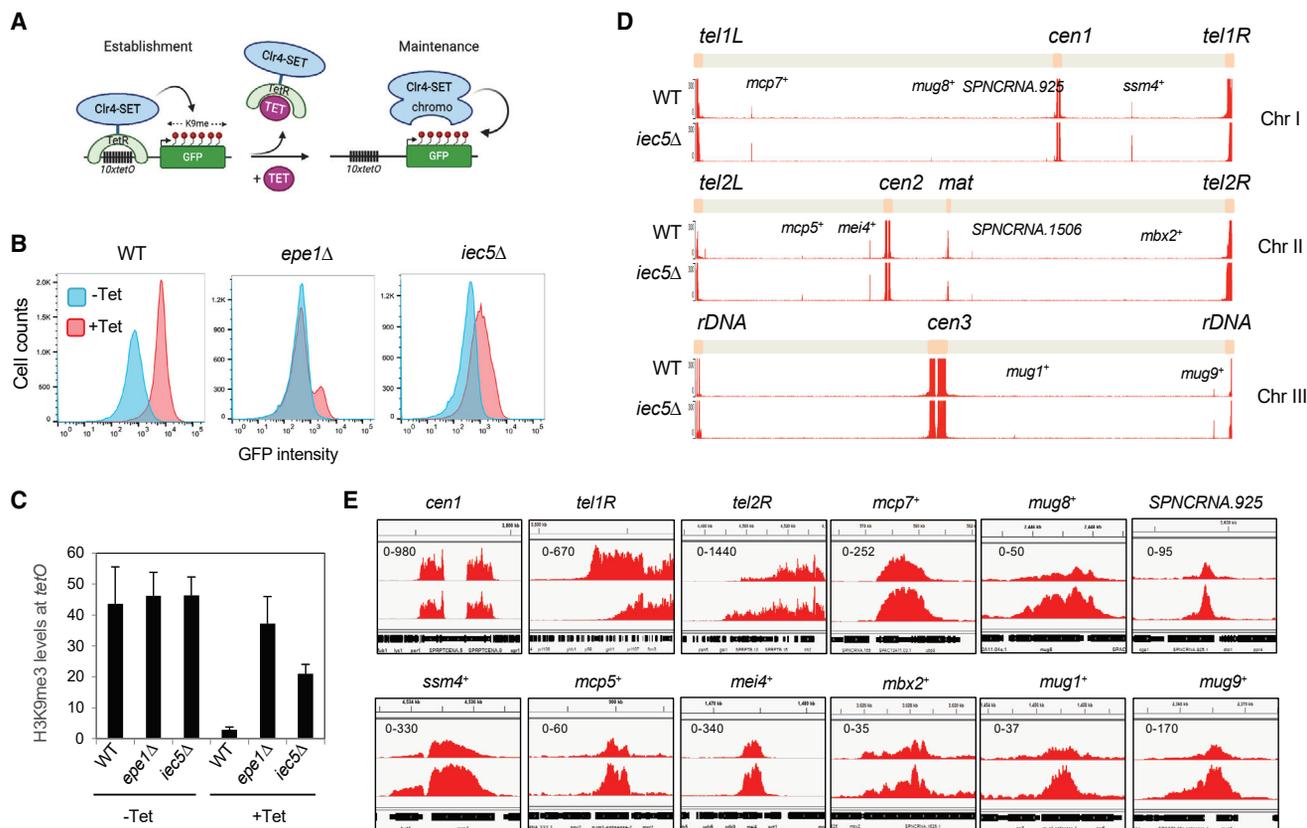
Figure 7. INO80 Is Required for Heterochromatin Inheritance and Maintenance of the Heterochromatin Landscape across the Genome

(A) Diagram of the TetR-Clr4-SET system. The targeting of the SET domain of Clr4 to *tetO* sites results in the formation of heterochromatin and the silencing of the adjacent *GFP*⁺ reporter gene. The addition of tetracycline (TET) results in the release of Clr4 from *tetO* sites, and heterochromatin is maintained by endogenous Clr4, which contains a chromodomain that recognizes H3K9me.

(B) FACS analyses of GFP expression before and 24 h after the addition of tetracycline.

(C) ChIP analysis of H3K9me3 levels at *tetO* before and 24 h after the addition of tetracycline, normalized to *act1*⁺. Data are presented as means ± SD, n = 3.

(D) Genome viewer representations of normalized ChIP-seq reads of H3K9me2 across the three chromosomes. Reads are normalized as CPMs.

(E) Examples of H3K9me2 ChIP-seq reads mapped to pericentric repeat regions of chromosome 1 (*cen1*), subtelomere 1, and heterochromatin islands. Reads are normalized as CPMs.

See also Figures S4–S6.

pericentric heterochromatin, suggesting the existence of mechanisms that counteract histone-based epigenetic inheritance (Reddy et al., 2011). As a result, RNAi is needed to consistently re-establish heterochromatin. Here, we show that mutations in the INO80 chromatin-remodeling complex allow heterochromatin inheritance even in the absence of RNAi-mediated heterochromatin establishment. INO80 mutations reduce histone turnover at heterochromatin, consistent with the fact that low histone turnover is critical for the preservation of heterochromatin structure (Aygün et al., 2013; Holla et al., 2020; Reddy et al., 2011; Sadeghi et al., 2015).

What then necessitates INO80 to localize at heterochromatin regions and to regulate histone turnover? The repeat regions are transcribed during the S phase of the cell cycle (Chen et al., 2008; Kloc et al., 2008), which inevitably leads to the collision of RNA polymerase II (Pol II) with the advancing replication fork (Zaratiegui et al., 2011). INO80 is critical for resolving transcription replication conflicts by removing Pol II (Lafon et al.,

2015; Poli et al., 2016). Therefore, the presence of INO80 at heterochromatin might be essential to ensure the proper replication of heterochromatin. However, an undesired effect is an increase in the histone turnover rate at heterochromatin regions, which reduces the amounts of modified histones on parental and daughter DNA strands, thereby affecting the prorogation of H3K9me required for heterochromatin inheritance (Figure 6F). The mechanism of how INO80 regulates histone turnover is not clear. It is highly likely that such a function requires the enzymatic activity of INO80. However, we could not directly test that idea because components critical for enzymatic activity are essential in fission yeast. The three core subunit mutants, *ies2Δ*, *ies4Δ*, and *arp8Δ*, are all viable and relatively healthy, and therefore, might only mildly affect INO80 activity *in vivo*.

INO80 not only regulates heterochromatin inheritance in RNAi mutants but also controls the stability of heterochromatin islands in wild-type cells. These heterochromatin islands frequently change under different environmental conditions or genetic

perturbations, and in certain cases, the formation of new heterochromatin islands allows cells to adapt to changes (Gallagher et al., 2018; Iglesias et al., 2018; Parsa et al., 2018; Sorida et al., 2019; Torres-Garcia et al., 2020; Wang et al., 2015; Zofall et al., 2012). Interestingly, INO80 is critical for regulating gene expression in response to diverse nutrient environments (Morrison, 2020). Therefore, the ability of INO80 to regulate heterochromatin islands might be part of the response for cells to adapt to the changing environmental conditions.

INO80 regulates diverse cellular processes, such as transcription, DNA replication, and DNA damage repair (Poli et al., 2017). However, the functions of INO80 in different biological processes are not well understood because of the lack of mutations that specifically abolish each function. We found that *iec5Δ* affects histone turnover, but not nucleosome positioning, at heterochromatin. Moreover, *iec5Δ* has little effect on transcription or DNA damage response. Therefore, *iec5Δ* provides a unique separation-of-function mutation that allows us to demonstrate the role of histone turnover in epigenetic inheritance. The molecular function of Iec5 is currently unknown. It has no obvious domain structure that can imply a function. We also generated recombinant Iec5 protein and found it does not interact with histones (data not shown). Therefore, it is unlikely to be a histone chaperone. Given that Iec5 preferentially regulates histone turnover at heterochromatin regions, it is likely that Iec5 interacts with some heterochromatin components to affect INO80 activity. It remains to be tested whether Iec5 directly affects INO80 enzymatic activity or regulates histone turnover through indirect mechanisms.

Subunits of the INO80 complex catalytic core are highly conserved (Morrison and Shen, 2009). Each species also contains several accessory subunits, which are more divergent. One possible explanation is that different organisms have evolved species-specific functions to adapt to their unique chromatin environment. However, we favor the possibility that the accessory subunits share conserved functions but are divergent at the sequence level. Indeed, we found sequence similarities between Iec5 and accessory INO80 subunits from other species and identified conserved residue that is required for Iec5 function. Interestingly, budding yeast INO80 also regulates the stability of heterochromatin (Xue et al., 2015). Therefore, it would be interesting to test whether the INO80 complex regulates the inheritance of epigenetic states in higher organisms.

STAR★METHODS

Detailed methods are provided in the online version of this paper and include the following:

- KEY RESOURCES TABLE
- RESOURCE AVAILABILITY
  - Lead Contact
  - Materials Availability
  - Data and Code Availability
- EXPERIMENTAL MODEL AND SUBJECT DETAILS
- METHOD DETAILS
  - Genetic screen with the fission yeast deletion library
  - Serial dilution analyses

- Protein purification, co-immunoprecipitation, and mass spectrometry analysis
- Chromatin immunoprecipitation (ChIP) analyses
- ChIP-seq
- MNase-seq
- RNA analyses
- RNA-seq
- FACS analysis
- QUANTIFICATION AND STATISTICAL ANALYSIS

AUTHOR CONTRIBUTIONS

C.-M.S., K.B., and S.J. designed and performed the experiments; J.D. and J.R.Y. performed mass spectrometry analyses; and X.C. and C.L. analyzed deep-sequencing data. S.J. and C.-M.S. wrote the manuscript with input from all authors.

DECLARATION OF INTERESTS

The authors declare no competing interests.

REFERENCES

Allshire, R.C., and Madhani, H.D. (2018). Ten principles of heterochromatin formation and function. Nat. Rev. Mol. Cell Biol. *19*, 229–244.

Allshire, R.C., Nimmo, E.R., Ekwall, K., Javerzat, J.P., and Cranston, G. (1995). Mutations derepressing silent centromeric domains in fission yeast disrupt chromosome segregation. Genes Dev. *9*, 218–233.

Audergon, P.N., Catania, S., Kagansky, A., Tong, P., Shukla, M., Pidoux, A.L., and Allshire, R.C. (2015). Epigenetics: restricted epigenetic inheritance of H3K9 methylation. Science *348*, 132–135.

Aygün, O., Mehta, S., and Grewal, S.I. (2013). HDAC-mediated suppression of histone turnover promotes epigenetic stability of heterochromatin. Nat. Struct. Mol. Biol. *20*, 547–554.

Bayne, E.H., White, S.A., Kagansky, A., Bijos, D.A., Sanchez-Pulido, L., Hoe, K.L., Kim, D.U., Park, H.O., Ponting, C.P., Rappsilber, J., and Allshire, R.C. (2010). Stc1: a critical link between RNAi and chromatin modification required for heterochromatin integrity. Cell *140*, 666–677.

Bernard, P., Maure, J.F., Partridge, J.F., Genier, S., Javerzat, J.P., and Allshire, R.C. (2001). Requirement of heterochromatin for cohesion at centromeres. Science *294*, 2539–2542.

Campos, E.I., Stafford, J.M., and Reinberg, D. (2014). Epigenetic inheritance: histone bookmarks across generations. Trends Cell Biol. *24*, 664–674.

Chen, E.S., Zhang, K., Nicolas, E., Cam, H.P., Zofall, M., and Grewal, S.I. (2008). Cell cycle control of centromeric repeat transcription and heterochromatin assembly. Nature *451*, 734–737.

Fischer, T., Cui, B., Dhakshnamoorthy, J., Zhou, M., Rubin, C., Zofall, M., Veenstra, T.D., and Grewal, S.I. (2009). Diverse roles of HP1 proteins in heterochromatin assembly and functions in fission yeast. Proc. Natl. Acad. Sci. USA *106*, 8998–9003.

Gallagher, P.S., Larkin, M., Thillainadesan, G., Dhakshnamoorthy, J., Balachandran, V., Xiao, H., Wellman, C., Chatterjee, R., Wheeler, D., and Grewal, S.I.S. (2018). Iron homeostasis regulates facultative heterochromatin assembly in adaptive genome control. Nat. Struct. Mol. Biol. *25*, 372–383.

Grewal, S.I., and Jia, S. (2007). Heterochromatin revisited. Nat. Rev. Genet. *8*, 35–46.

Grewal, S.I., and Klar, A.J. (1996). Chromosomal inheritance of epigenetic states in fission yeast during mitosis and meiosis. Cell *86*, 95–101.

Hall, I.M., Shankaranarayana, G.D., Noma, K., Ayoub, N., Cohen, A., and Grewal, S.I. (2002). Establishment and maintenance of a heterochromatin domain. Science *297*, 2232–2237.

Hall, I.M., Noma, K., and Grewal, S.I. (2003). RNA interference machinery regulates chromosome dynamics during mitosis and meiosis in fission yeast. Proc. Natl. Acad. Sci. USA *100*, 193–198.

Hogan, C.J., Aligianni, S., Durand-Dubief, M., Persson, J., Will, W.R., Webster, J., Wheeler, L., Mathews, C.K., Elderkin, S., Oxley, D., et al. (2010). Fission yeast Iec1-ino80-mediated nucleosome eviction regulates nucleotide and phosphate metabolism. Mol. Cell. Biol. *30*, 657–674.

Holla, S., Dhakshnamoorthy, J., Folco, H.D., Balachandran, V., Xiao, H., Sun, L.L., Wheeler, D., Zofall, M., and Grewal, S.I.S. (2020). Positioning heterochromatin at the nuclear periphery suppresses histone turnover to promote epigenetic inheritance. Cell *180*, 150–164.e115.

Hou, H., Wang, Y., Kallgren, S.P., Thompson, J., Yates, J.R., 3rd, and Jia, S. (2010). Histone variant H2A.Z regulates centromere silencing and chromosome segregation in fission yeast. J. Biol. Chem. *285*, 1909–1918.

Iglesias, N., Currie, M.A., Jih, G., Paulo, J.A., Siuti, N., Kalocsay, M., Gygi, S.P., and Moazed, D. (2018). Automethylation-induced conformational switch in Clr4 (Suv39h) maintains epigenetic stability. Nature *560*, 504–508.

Iglesias, N., Paulo, J.A., Tatarakis, A., Wang, X., Edwards, A.L., Bhanu, N.V., Garcia, B.A., Haas, W., Gygi, S.P., and Moazed, D. (2020). Native chromatin proteomics reveals a role for specific nucleoporins in heterochromatin organization and maintenance. Mol. Cell. *77*, 51–66.e58.

Jia, S., Noma, K., and Grewal, S.I. (2004). RNAi-independent heterochromatin nucleation by the stress-activated ATF/CREB family proteins. Science *304*, 1971–1976.

Kagansky, A., Folco, H.D., Almeida, R., Pidoux, A.L., Boukaba, A., Simmer, F., Urano, T., Hamilton, G.L., and Allshire, R.C. (2009). Synthetic heterochromatin bypasses RNAi and centromeric repeats to establish functional centromeres. Science *324*, 1716–1719.

Kim, D., Langmead, B., and Salzberg, S.L. (2015). HISAT: a fast spliced aligner with low memory requirements. Nat. Methods *12*, 357–360.

Kloc, A., Zaratiegui, M., Nora, E., and Martienssen, R. (2008). RNA interference guides histone modification during the S phase of chromosomal replication. Curr. Biol. *18*, 490–495.

Krietenstein, N., Wal, M., Watanabe, S., Park, B., Peterson, C.L., Pugh, B.F., and Korber, P. (2016). Genomic nucleosome organization reconstituted with pure proteins. Cell *167*, 709–721.e12.

Lafon, A., Taranum, S., Pietrocola, F., Dingli, F., Loew, D., Brahma, S., Bartholomew, B., and Papamichos-Chronakis, M. (2015). INO80 chromatin remodeler facilitates release of RNA polymerase II from chromatin for ubiquitin-mediated proteasomal degradation. Mol. Cell *60*, 784–796.

Langmead, B., Trapnell, C., Pop, M., and Salzberg, S.L. (2009). Ultrafast and memory-efficient alignment of short DNA sequences to the human genome. Genome Biol. *10*, R25.

Liao, Y., Smyth, G.K., and Shi, W. (2014). featureCounts: an efficient general purpose program for assigning sequence reads to genomic features. Bioinformatics *30*, 923–930.

Lock, A., Rutherford, K., Harris, M.A., Hayles, J., Oliver, S.G., Bähler, J., and Wood, V. (2019). PomBase 2018: user-driven reimplementation of the fission yeast database provides rapid and intuitive access to diverse, interconnected information. Nucleic Acids Res. *47* (*D1*), D821–D827.

Love, M.I., Huber, W., and Anders, S. (2014). Moderated estimation of fold change and dispersion for RNA-seq data with DESeq2. Genome Biol. *15*, 550.

Martienssen, R., and Moazed, D. (2015). RNAi and heterochromatin assembly. Cold Spring Harb. Perspect. Biol. *7*, a019323.

Mizuguchi, G., Shen, X., Landry, J., Wu, W.H., Sen, S., and Wu, C. (2004). ATP-driven exchange of histone H2AZ variant catalyzed by SWR1 chromatin remodeling complex. Science *303*, 343–348.

Moazed, D. (2011). Mechanisms for the inheritance of chromatin states. Cell *146*, 510–518.

Morrison, A.J. (2020). Chromatin-remodeling links metabolic signaling to gene expression. Mol. Metab. *38*, 100973.

Morrison, A.J., and Shen, X. (2009). Chromatin remodelling beyond transcription: the INO80 and SWR1 complexes. Nat. Rev. Mol. Cell Biol. *10*, 373–384.

Motamedi, M.R., Hong, E.J., Li, X., Gerber, S., Denison, C., Gygi, S., and Moazed, D. (2008). HP1 proteins form distinct complexes and mediate heterochromatic gene silencing by nonoverlapping mechanisms. Mol. Cell *32*, 778–790.

Nakayama, J., Rice, J.C., Strahl, B.D., Allis, C.D., and Grewal, S.I. (2001). Role of histone H3 lysine 9 methylation in epigenetic control of heterochromatin assembly. Science *292*, 110–113.

Nonaka, N., Kitajima, T., Yokobayashi, S., Xiao, G., Yamamoto, M., Grewal, S.I., and Watanabe, Y. (2002). Recruitment of cohesin to heterochromatic regions by Swi6/HP1 in fission yeast. Nat. Cell Biol. *4*, 89–93.

Parsa, J.Y., Boudoukha, S., Burke, J., Homer, C., and Madhani, H.D. (2018). Polymerase pausing induced by sequence-specific RNA-binding protein drives heterochromatin assembly. Genes Dev. *32*, 953–964.

Poli, J., Gerhold, C.B., Tosi, A., Hustedt, N., Seeber, A., Sack, R., Herzog, F., Pasero, P., Shimada, K., Hopfner, K.P., and Gasser, S.M. (2016). Mec1, INO80, and the PAF1 complex cooperate to limit transcription replication conflicts through RNAPII removal during replication stress. Genes Dev. *30*, 337–354.

Poli, J., Gasser, S.M., and Papamichos-Chronakis, M. (2017). The INO80 remodeller in transcription, replication and repair. Philos. Trans. R. Soc. Lond. B Biol. Sci. *372*, 201160290.

Ragunathan, K., Jih, G., and Moazed, D. (2014). Epigenetic inheritance uncoupled from sequence-specific recruitment. Science *348*, 1258699.

Raiymbek, G., An, S., Khurana, N., Gopinath, S., Larkin, A., Biswas, S., Trievel, R.C., Cho, U.S., and Ragunathan, K. (2020). An H3K9 methylation-dependent protein interaction regulates the non-enzymatic functions of a putative histone demethylase. eLife *9*, e53155.

Ramírez, F., Ryan, D.P., Grüning, B., Bhardwaj, V., Kilpert, F., Richter, A.S., Heyne, S., Dündar, F., and Manke, T. (2016). deepTools2: a next generation web server for deep-sequencing data analysis. Nucleic Acids Res. *44*, W160–W165.

Rea, S., Eisenhaber, F., O'Carroll, D., Strahl, B.D., Sun, Z.W., Schmid, M., Opravil, S., Mechtler, K., Ponting, C.P., Allis, C.D., and Jenuwein, T. (2000). Regulation of chromatin structure by site-specific histone H3 methyltransferases. Nature *406*, 593–599.

Reddy, B.D., Wang, Y., Niu, L., Higuchi, E.C., Marguerat, S.B., Bähler, J., Smith, G.R., and Jia, S. (2011). Elimination of a specific histone H3K14 acetyltransferase complex bypasses the RNAi pathway to regulate pericentric heterochromatin functions. Genes Dev. *25*, 214–219.

Robinson, J.T., Thorvaldsdóttir, H., Winckler, W., Guttman, M., Lander, E.S., Getz, G., and Mesirov, J.P. (2011). Integrative genomics viewer. Nat. Biotechnol. *29*, 24–26.

Roguev, A., Wiren, M., Weissman, J.S., and Krogan, N.J. (2007). High-throughput genetic interaction mapping in the fission yeast *Schizosaccharomyces pombe*. Nat. Methods *4*, 861–866.

Rothbauer, U., Zolghadr, K., Muyldermans, S., Schepers, A., Cardoso, M.C., and Leonhardt, H. (2008). A versatile nanotrap for biochemical and functional studies with fluorescent fusion proteins. Mol. Cell. Proteomics *7*, 282–289.

Sadeghi, L., Prasad, P., Ekwall, K., Cohen, A., and Svensson, J.P. (2015). The Paf1 complex factors Leo1 and Paf1 promote local histone turnover to modulate chromatin states in fission yeast. EMBO Rep. *16*, 1673–1687.

Serra-Cardona, A., and Zhang, Z. (2018). Replication-coupled nucleosome assembly in the passage of epigenetic information and cell identity. Trends Biochem. Sci. *43*, 136–148.

Singh, P.P., Shukla, M., White, S.A., Lafos, M., Tong, P., Auchynnikava, T., Spanos, C., Rappsilber, J., Pidoux, A.L., and Allshire, R.C. (2020). Hap2-Ino80-facilitated transcription promotes de novo establishment of CENP-A chromatin. Genes Dev. *34*, 226–238.

Sorida, M., Hirauchi, T., Ishizaki, H., Kaito, W., Shimada, A., Mori, C., Chikashige, Y., Hiraoka, Y., Suzuki, Y., Ohkawa, Y., et al. (2019). Regulation of ectopic heterochromatin-mediated epigenetic diversification by the JmjC family protein Epe1. PLoS Genet. *15*, e1008129.

Stewart-Morgan, K.R., Petryk, N., and Groth, A. (2020). Chromatin replication and epigenetic cell memory. Nat. Cell Biol. *22*, 361–371.

Tadeo, X., Wang, J., Kallgren, S.P., Liu, J., Reddy, B.D., Qiao, F., and Jia, S. (2013). Elimination of shelterin components bypasses RNAi for pericentric heterochromatin assembly. Genes Dev. *27*, 2489–2499.

Torres-Garcia, S., Yaseen, I., Shukla, M., Audergon, P.N.C.B., White, S.A., Pidoux, A.L., and Allshire, R.C. (2020). Epigenetic gene silencing by heterochromatin primes fungal resistance. Nature *585*, 453–458.

Udugama, M., Sabri, A., and Bartholomew, B. (2011). The INO80 ATP-dependent chromatin remodeling complex is a nucleosome spacing factor. Mol. Cell. Biol. *31*, 662–673.

Valouev, A., Johnson, S.M., Boyd, S.D., Smith, C.L., Fire, A.Z., and Sidow, A. (2011). Determinants of nucleosome organization in primary human cells. Nature *474*, 516–520.

Volpe, T., Schramke, V., Hamilton, G.L., White, S.A., Teng, G., Martienssen, R.A., and Allshire, R.C. (2003). RNA interference is required for normal centromere function in fission yeast. Chromosome Res. *11*, 137–146.

Wang, X., and Moazed, D. (2017). DNA sequence-dependent epigenetic inheritance of gene silencing and histone H3K9 methylation. Science *356*, 88–91.

Wang, J., Reddy, B.D., and Jia, S. (2015). Rapid epigenetic adaptation to uncontrolled heterochromatin spreading. eLife *4*, e06179.

Wickham, H., Navarro, D., and Pedersen, T.L. (2016). ggplot2: Elegant Graphics for Data Analysis. (Springer-Verlag).

Xue, Y., Van, C., Pradhan, S.K., Su, T., Gehrke, J., Kuryan, B.G., Kitada, T., Vashisht, A., Tran, N., Wohlschlegel, J., et al. (2015). The Ino80 complex prevents invasion of euchromatin into silent chromatin. Genes Dev. *29*, 350–355.

Yen, K., Vinayachandran, V., Batta, K., Koerber, R.T., and Pugh, B.F. (2012). Genome-wide nucleosome specificity and directionality of chromatin remodelers. Cell *149*, 1461–1473.

Yen, K., Vinayachandran, V., and Pugh, B.F. (2013). SWR-C and INO80 chromatin remodelers recognize nucleosome-free regions near +1 nucleosomes. Cell *154*, 1246–1256.

Zaratiegui, M., Castel, S.E., Irvine, D.V., Kloc, A., Ren, J., Li, F., de Castro, E., Marín, L., Chang, A.Y., Goto, D., et al. (2011). RNAi promotes heterochromatic silencing through replication-coupled release of RNA Pol II. Nature *479*, 135–138.

Zhang, K., Mosch, K., Fischle, W., and Grewal, S.I. (2008). Roles of the Clr4 methyltransferase complex in nucleation, spreading and maintenance of heterochromatin. Nat. Struct. Mol. Biol. *15*, 381–388.

Zofall, M., Fischer, T., Zhang, K., Zhou, M., Cui, B., Veenstra, T.D., and Grewal, S.I. (2009). Histone H2A.Z cooperates with RNAi and heterochromatin factors to suppress antisense RNAs. Nature *461*, 419–422.

Zofall, M., Yamanaka, S., Reyes-Turcu, F.E., Zhang, K., Rubin, C., and Grewal, S.I. (2012). RNA elimination machinery targeting meiotic mRNAs promotes facultative heterochromatin formation. Science *335*, 96–100.

STAR★METHODS

KEY RESOURCES TABLE

REAGENT or RESOURCE	SOURCE	IDENTIFIER
Antibodies		
Mouse monoclonal anti-FLAG	Sigma	Cat#F3165; RRID:AB_259529
Rabbit Polyclonal anti-c-Myc (A-14)	Santa Cruz Biotechnology	Cat#sc-789; RRID:AB_631274
Rabbit Polyclonal anti-Swi6	This paper	N/A
Rabbit Polyclonal anti-H3K9me3	Active Motif	Cat# 39161, RRID:AB_2532132
Rabbit Polyclonal anti-H3K9me2	Abcam	Cat#ab115159, RRID: AB_1090318
Anti-Tubulin	Keith Gull lab	N/A
Anti-flag M2 affinity gel	Sigma	Cat# A2220, RRID:AB_10063035
Chemicals, Peptides, and Recombinant Proteins		
Formaldehyde, 37% solution	Sigma	Cat#F8775
Tris(2-Carboxyethyl)-Phosphine Hydrochloride	Sigma	Cat#C4706
5-Fluoroorotic Acid Monohydrate (FOA, 5-FOA)	US Biological	Cat#F5050
RNase A	Thermo Fisher Scientific	Cat#EN0531
MNase	Thermo Fisher Scientific	Cat#88216
Proteinase K	Invitrogen	Cat#10005393
Phenol-chloroform-isoamyl alcohol mixture	Sigma	Cat#77617
Thiabendazole (TBZ)	Sigma	Cat#T5535
Tetracycline	Sigma	Cat#87128
Geneticin (G418)	GIBCO	Cat#11811-098
Nourseothricin Sulfate	Gold Biotechnology	Cat#N-500-1
Hygromycin B	Gold Biotechnology	Cat#H-270-10
EMM Powder	Sunrise Science Products	Cat#2005-1KG
Hydroxyurea	Sigma	Cat#H8627
Cycloheximide	Sigma	Cat#01810
Bleomycin Sulfate	Sigma	Cat#B5507
Critical Commercial Assays		
RiboMinus Transcriptome Isolation Kit	ThermoFisher Scientific	Cat#K155003
NEBNext® Ultra II Directional RNA Library Prep Kit for Illumina	New England Biolabs	Cat#E7760
Power SYBR Green RNA-to-CT one-step Kit	Applied Biosystems	Cat#4389986
MasterPure yeast RNA purification kit	Epicenter	Cat# MPY03100
Qubit dsDNA HS Assay Kit	Thermo Fisher Scientific	Cat#Q33230
Maxima SYBR Green qPCR Master Mix	ThermoFisher Scientific	Cat#K0223
Deposited Data		
Sequencing Data	This paper	GEO: GSE150545
Experimental Models: Organisms/Strains		
S. pombe strains, see Table S7	This paper	N/A
Fission yeast deletion library	Bioneer	Cat#2030H
Oligonucleotides		
Primers, see Table S8	This paper	N/A
Software and Algorithms		
HISAT2	UT Southwestern (Kim Lab)	v2.1.0
FACSDiva	Becton, Dickinson and Company	v2.1.0
FlowJo	Becton, Dickinson and Company	v10.6.2

(Continued on next page)

Continued		
REAGENT or RESOURCE	SOURCE	IDENTIFIER
Picard	Broad Institute MIT	v2.22.0
DeepTools	Max Planck Institute	v3.3.2
DTASelect	The Scripps Research Institute (Yates Lab)	v2.0
ProLuCID	The Scripps Research Institute (Yates Lab)	v1.3

RESOURCE AVAILABILITY

Lead Contact
Further information and request for resources and reagents should be directed to and will be fulfilled by the Lead Contact, Songtao Jia (songtao.jia@columbia.edu).

Materials Availability
The materials generated in this study is available upon request and will be shared without restriction.

Data and Code Availability
The accession number for the RNA-seq, MNase-seq, and ChIP-seq data reported in this paper are GEO: GSE150545.

EXPERIMENTAL MODEL AND SUBJECT DETAILS

A list of fission yeast strains used in this study is provided in Table S7. Yeast strains containing *ino80$^+$-Flag*, *iec1$^+$-Flag*, *hap2$^+$-Flag*, *nht1$^+$-Flag*, *iec3$^+$-Flag*, *iec5$^+$-Flag*, *iec5$^+$-myc*, *iec5$^+$-GFP*, *iec1$^+$-GBP*, *nht1$^+$-myc*, *iec3Δ*, or *iec5Δ* were generated by a PCR-based module method. Epitope tags are integrated at the endogenous genetic loci and tagged genes are under the control of their native promoters. Deletion strains *iec1Δ*, *hap2Δ*, *nht1Δ*, *ies2Δ*, *ies4Δ*, *arp8Δ* were derived from the fission yeast deletion library, and the gene deletions were verified by PCR analyses and DNA sequencing. All other strains were constructed through genetic crosses.

METHOD DETAILS

Genetic screen with the fission yeast deletion library
The genetic screen for mutations that alleviate silencing defects of *dcr1Δ* was performed as previously described (Roguev et al., 2007). The fission yeast deletion library (Bioneer) was constructed by replacing individual genes with a *KanMX4* cassette that confers resistance to geneticin. The *otr::ura4$^+$* query strain was constructed by inserting a *NatMX6* cassette, which confers resistance to nourseothricin, ~400 bp to the right side boundary of centromere I heterochromatin. The *otr::ura4$^+$* reporter was introduced into the deletion library first, followed by the introduction of *dcr1Δ*, using the RoToR HDA pinning robot (Singer). After mating, haploid progeny of desired genotypes were selected by a combination of antibiotics. The colonies were then pinned onto FOA plates to measure colony growth.

Serial dilution analyses
For serial dilution plating assays, ten-fold dilutions of a mid log-phase culture were plated on the indicated medium and grown for 3 days at 30°C.

Protein purification, co-immunoprecipitation, and mass spectrometry analysis
Log phase yeast cells were harvested and washed with 2xHC buffer (300 mM HEPES-KOH at pH 7.6, 2 mM EDTA, 100 mM KCl, 20% glycerol, 2 mM DTT, 1mM PMSF) and frozen in liquid nitrogen. Crude cell extracts were prepared by vigorously blending frozen yeast cells with dry ice using a household blender, followed by incubation with 1xHC buffer containing 250 mM KCl for 30 minutes. The lysate was cleared by centrifugation at 20,000 g for 1 hour. The supernatants were incubated with Flag-agarose (Sigma) overnight, and washed eight times with 1xHC containing 250 mM KCl. For mass spectrometry analysis, bound proteins were eluted with 3xFlag peptides followed by TCA precipitation.

For co-immunoprecipitation analysis, bound proteins were resolved by SDS-PAGE followed by western blot analyses with Myc (Santa Cruz Biotechnology), or Flag (Sigma) antibodies.

For mass spectrometry analyses, protein pellets were dissolved in buffer (8 M urea, 100 mM Tris pH 8.5), reduced with TCEP (Tris [2-Carboxyethyl]-Phosphine Hydrochloride), and alklyated with chloroacetamide. After dilution of urea to 2 M, proteins were digested with trypsin. Digested peptides were analyzed by LC/LC/MS/MS using an LTQ mass spectrometer. Multidimensional chromatography was performed online with 6 salt steps. Tandem mass spectra were collected in a data-dependent manner with up to

5 ms2 scans performed for each initial scan (m/z range 300-2000). The search program Prolucid was used to match data to a fission yeast protein database. Peptide identifications were filtered using the DTASelect program.

Chromatin immunoprecipitation (ChIP) analyses

Log-phase yeast cells grown at 30°C were incubated at 18°C for 2 hours and then fixed for 30 minutes in 3% freshly made formaldehyde. The cells were pelleted and washed with PBS (phosphate-buffered saline) before resuspended in ChIP lysis buffer (50 mM HEPES-KOH, pH 7.5, 140 mM NaCl, 1% Triton X-100, 0.1% Deoxycholate). Ice cold glass beads were added, and the mixtures were vigorously disrupted in a beadbeater. The lysates were collected and subjected to sonication to reduce chromatin size to 500-1000 base pairs (bp). The cleared cell lysates were incubated with Flag-agarose beads (Sigma) overnight at 4°C. The beads were then washed with ChIP lysis buffer twice, ChIP lysis buffer containing 0.5 M NaCl, Wash buffer (10 mM Tris, pH 8.0, 250 mM LiCl, 0.5% NP-40, 0.5% Deoxycholate, 1 mM EDTA), and TE (50 mM Tris pH 8.0, 1 mM EDTA). The bound chromatin fragments were eluted with TES (50 mM Tris pH 8.0, 1 mM EDTA, 1% SDS) and the crosslinking was reversed by incubating at 65°C overnight. The protein DNA mixture was then subjected to proteinase K treatment and phenol:chloroform extraction before the DNA was precipitated by ethanol.

For histone turnover assay, cells were cultured in EMM-uracil medium, and then arrested for four hours by 11 mM HU, followed by the addition of 0.25 mg/mL uracil to induce the expression of H3-Flag for 1 hour, before ChIP analysis was performed.

Quantitative real-time PCR (qPCR) was performed with Maxima SYBR Green qPCR Master Mix (Fermentas) in a StepOne Plus Real-Time PCR System (Applied Biosystems). DNA serial dilutions were used as templates to generate a standard curve of amplification for each pair of primers, and the relative concentration of the target sequence was calculated accordingly. An *act1* fragment was used to calculate the enrichment of ChIP over whole cell extract (WCE) for each target sequence when indicated.

ChIP-seq

Log-phase yeast cells were crosslinked with 1% formaldehyde for 20 minutes with shaking at room temperature, followed by 5 minutes quenching with 125mM glycine. Cells were harvested, washed with PBS (phosphate-buffered saline), and resuspended in ChIP lysis buffer (50 mM HEPES-KOH, pH 7.5, 140 mM NaCl, 1% Triton X-100, 0.1% Deoxycholate, 1mM PMSF). Ice-cold glass beads were added and the mixtures were vigorously disrupted in a bead-beater with four 30 s rounds. The lysates were collected and NP buffer was added (10 mM Tris, pH 7.4, 1 M sorbitol, 50 mM NaCl, 5 mM MgCl$_2$, 1 mM CaCl$_2$). MNase was added to the reaction and the reactions were incubated at 37°C for 20 minutes. MNase amount was titrated empirically so that the chromatin was digested to yield mainly mono- and di-nucleosomes. The reaction was stopped by the addition of 0.5 M EDTA, and the tubes were placed on ice. 5X ChIP lysis buffer was added to the reaction, mixed by short vortexing, and the tubes were incubated on ice for 30 minutes. The reactions were then cleared by centrifugation at 16,000 x *g* for 10 minutes. A small fraction of the cleared supernatant was reserved as input and the rest was used for immunoprecipitation. The protocols for immunoprecipitation, reverse-crosslinking, and DNA precipitation are the same as in the previous ChIP section. The precipitated DNA was treated with RNAase A (EN0531, Thermo Fisher Scientific) for 1 hour at 37°C. DNA concentration was determined with the Qubit dsDNA HS Assay Kit (Q33230, Thermo Fisher Scientific). 5-10 ng of ChIP and input DNA were used for library construction using the NEBNext Ultra II DNA Library Prep Kit for Illumina (E7645, NEB). Libraries were pooled and sequenced on a NextSeq500/550 with the Mid-output kit (150 cycles, single-end) at the JP Sulzberger Genome Center at Columbia University.

Sequencing reads were de-multiplexed and aligned to the *S. pombe* reference genome, obtained from Pombase (Lock et al., 2019) with Bowtie using default parameters (Langmead et al., 2009). Genome-wide coverage was calculated with deepTools2 (Ramírez et al., 2016) and normalized to counts per million (CPM). The coverage plot was visualized with IGV (Robinson et al., 2011). ChIP-seq experiments were performed in duplicates for each genotype.

MNase-seq

MNase-seq sample preparation was the same as the ChIP-seq except that MNase was titrated to yield mainly mononucleosomes (∼80% mono-nucleosomes) and the immunoprecipitation step was omitted. 100 ng of extracted DNA was used for library construction as above. Libraries were pooled and sequenced on a NextSeq500/550 with the Mid-output kit (150 cycles, pair-end) at the JP Sulzberger Genome Center at Columbia University. MNase-seq experiments were performed in duplicates for each genotype.

MNase-seq reads of each sample were mapped to the genome assembly of *Schizosaccharomyces pombe* using HISAT2 (v2.1.0) (Kim et al., 2015). Potential PCR duplicates were removed using the function "MarkDuplicates" of Picard (http://broadinstitute.github.io/picard/ v2.22.0, REMOVE_DUPLICATES = true). The fragment size distribution was measured by the function "CollectInsertSizeMetrics" of Picard (v2.22.0). Only mono-nucleosome sized fragments (< 200 bp) were used for the downstream analysis. Nucleosome periodicity in the MNase-seq data was calculated by phasogram (Valouev et al., 2011) using either all fragment centers across the genome or fragment centers on pericentromeric regions. The nucleosome distribution in the promoter and pericentromeric regions are measured and visualized by the functions "computeMatrix" and "plotProfile" of deepTools (v 3.3.2) (Ramírez et al., 2016).

RNA analyses

Total cellular RNA was isolated from log-phase cells using MasterPure yeast RNA purification kit (Epicenter) according to the manufacturer's protocol. Quantification with real-time RT-PCR was performed with Power SYBR Green RNA-to-CT one-step Kit (Applied

Biosystems). RNA serial dilutions were used as templates to generate a standard curve of amplification for each pair of primers, and the relative concentration of the target sequence was calculated accordingly. An *act1* fragment served as a reference to normalize the concentration of samples. The concentration of each target gene in wild-type was arbitrarily set to 1 and served as a reference for other samples.

RNA-seq

For RNA-seq, the total RNA was treated with RiboMinus Transcriptome Isolation Kit (ThermoFisher Scientific, K155003) to deplete rRNA. The rRNA-depleted samples were used to construct strand-specific sequencing libraries with the NEBNext® Ultra II Directional RNA Library Prep Kit for Illumina® (NEB, E7760). Libraries were pooled and sequenced on a NextSeq500/550 with the Mid-output kit (150 cycles, pair-end) at the JP Sulzberger Genome Center at Columbia University. RNA-seq experiments were performed in duplicates for each genotype.

RNA-seq reads of each sample were mapped to the genome assembly of *Schizosaccharomyces pombe* using HISAT2 (v2.1.0) (Kim et al., 2015). The mapped reads count of each gene was measured by featureCounts (v1.6.1) (Liao et al., 2014). The differential gene expression was calculated and visualized by the R packages DESeq2 (v1.28.0) (Love et al., 2014) and ggplot2 (v3.2.1) (Wickham et al., 2016).

FACS analysis

Cells containing TetR-Clr4-SET and tetO-ura4-GFP reporter were cultured and kept in logarithm phase, and were harvested at various time points after the addition of tetracycline (2.5mg/ml). Cells were collected and fixed by the addition of 70% ethanol for 20 minutes. The cells were then washed twice with PBS (10 mM Na_2HPO_4, 1.8mM KH_2PO_4, pH 7.4, 137 mM NaCl, 2.7mM KCl), and resuspended in a FACS tube (BD Falcon). GFP fluorescence was measured using FACSCelesta (Becton Dickinson), and excitation was achieved by using an argon laser emission of 488 nm. Data collection was performed using Cellquest (Becton Dickinson), and a primary gate based on physical parameters (forward and side light scatter) was set to exclude dead cells or debris. Typically, 50,000 cells were analyzed for each sample and time point. Raw data were processed and histograms were drawn using FlowJo (10.6.2, Becton Dickinson).

QUANTIFICATION AND STATISTICAL ANALYSIS

For RNA-seq, FDR adjusted p values (q-values) were generated using the DEseq2 package (v1.28.0) in R. Significantly differentiated genes were defined as having over 2-fold change and a q-value < 0.1. For ChIP-qPCR and RT-qPCR, data are presented as mean ± SD and n represents number of replicates.